Deng et al. *Zool. Res.* 2025, 46(2): 263−276
https://doi.org/10.24272/j.issn.2095-8137.2024.286
https://cstr.cn/32248.14.zr.2024.286

ZR | Zoological Research

Article Open Access

# Ribosome-associated pathological TDP-43 alters the expression of multiple mRNAs in the monkey brain

Fu-Yu Deng[1,2], Gao-Lu Zhu[1], Kai-Li Ou[1], Long-Hong Zhu[1], Qing-Qing Jia[1], Xiang Wang[1], Ming-Wei Guo[1], Bang Li[1], Shi-Hua Li[1], Xiao-Jiang Li[1,*], Peng Yin[1,*]

[1] *Guangdong Key Laboratory of Non-human Primate Research*, *Ministry of Education Key Laboratory of CNS Regeneration*, *Guangdong-Hongkong-Macau Institute of CNS Regeneration*, *Jinan University*, *Guangzhou*, *Guangdong* 510632, *China*

[2] *Shenzhen Institute for Drug Control*, *Shenzhen Testing Center of Medical Devices*, *In vitro Diagnostic Reagents Testing Department*, *Shenzhen*, *Guangdong* 518057, *China*

## ABSTRACT

Cytoplasmic accumulation of TDP-43 is a pathological hallmark of amyotrophic lateral sclerosis (ALS) and other neurodegenerative diseases. While current studies have primarily focused on gene regulation mediated by full-length nuclear TDP-43, the potential effects of cytoplasmic TDP-43 fragments remain less explored. Our previous findings demonstrated that primate-specific cleavage of TDP-43 contributes to its cytoplasmic localization, prompting further investigation into its pathological effects. In the cynomolgus monkey brain, we observed that mutant or truncated TDP-43 was transported onto the ribosome organelle. Ribosome-associated transcriptomic analysis revealed dysregulation of apoptosis- and lysosome-related genes, indicating that cytoplasmic TDP-43 induces neurotoxicity by binding to ribosomes and disrupting mRNA expression. These findings provide mechanistic insights into the gain-of-function effects of pathological TDP-43.

**Keywords:** TDP-43; Ribosomes; Gain-of-function; Non-human primates

## INTRODUCTION

The nuclear TAR DNA/RNA binding protein 43 (TDP-43) regulates DNA transcription, RNA splicing, stability, and translation, playing a crucial role in various physiological functions (Chen-Plotkin et al., 2010; Cohen et al., 2011; Guo & Shorter, 2017; Lee et al., 2012; Polymenidou et al., 2011). Originally identified in postmortem samples from individuals with amyotrophic lateral sclerosis (ALS) and frontotemporal lobar degeneration (FTLD) (Neumann et al., 2006), TDP-43 pathology has since been observed in the brains of individuals with other neurodegenerative diseases, including Alzheimer's disease (AD), Lewy body dementia (LBD), and Huntington's disease (HD) (Kwong et al., 2007; Neumann et al., 2007; Winton et al., 2008). Over 50 TDP-43 mutations linked to ALS/FTLD have been identified, reinforcing its pathogenic role (Buratti, 2015; Watanabe et al., 2020). Structurally, TDP-43 contains two conserved RNA recognition motifs (RRM1 and RRM2) that mediate its binding to nucleic acids, facilitating its function in gene transcription and RNA processing (Buratti et al., 2005; Freibaum et al., 2010; Prakash et al., 2021). A defining characteristic of TDP-43 pathology is the accumulation of cytoplasmic aggregates coupled with nuclear depletion, suggesting that both gain- and loss-of-function mechanisms contribute to disease pathogenesis (Broeck et al., 2014; Kabashi et al., 2010; Lee et al., 2012; Xu & Yang, 2014). Current studies have primarily focused on manipulating TDP-43 function in the nucleus, either by suppressing normal protein levels or overexpressing TDP-43 in the nucleus to influence gene processing. However, relatively limited attention has been directed toward the pathological consequences of cytoplasmic TDP-43 accumulation, including its impact on gene regulation and subcellular mislocalization. This research gap is partially attributable to limitations in mouse models, which, despite their utility in recapitulating certain pathologies and mechanisms, fail to replicate the full spectrum of TDP-43 proteinopathy observed in human neurodegeneration. Cytoplasmic TDP-43 inclusions are a hallmark feature in ALS brains (Lagier-Tourenne & Cleveland, 2009; Neumann et al., 2006), yet most transgenic rodent models predominantly display nuclear localization of mutant TDP-43 (Gendron et al., 2013; Huang et al., 2012; Ni et al., 2023; Shan et al., 2010; Watanabe et al., 2020; Wegorzewska et al., 2009; Yan et al., 2014), with minimal cytoplasmic mislocalization (Janssens et al., 2013; Mitchell et al., 2015;



Received: 03 September 2024; Accepted: 03 December 2024; Online: 04 December 2024

Foundation items: This work was supported by the National Natural Science Foundation of China (32270564 to P.Y., 82394422 to X.J.L., 82371178 to B.L.) and Guangdong Basic and Applied Basic Research (2022A1515011205 and 2023A1515010811 to P.Y., 2021ZT09Y007 and 2018B030337001 to X.J.L.)

*Corresponding authors, E-mail: xjli33@jnu.edu.cn; yinpeng177@163.com

Wegorzewska et al., 2009; Wils et al., 2010). Furthermore, increasing evidence indicates that TDP-43 C-terminal fragment (CTF) expression fails to effectively replicate the progressive neuronal dysfunction and degeneration observed in patients, with rodent models expressing TDP-43 CTFs generally lacking extensive neurodegeneration or cell death (Caccamo et al., 2012; Dayton et al., 2013; Spiller et al., 2018). Consistently, studies in *Drosophila* have repeatedly demonstrated that full-length TDP-43 or disease-associated mutants elicit greater toxicity in retinal and neuronal cells than CTFs (Gregory et al., 2012; Li et al., 2010; Voigt et al., 2010). In contrast, large-animal models, such as monkeys (Jackson et al., 2015; Uchida et al., 2012; Yin et al., 2019) and pigs (Wang et al., 2015), provide a more physiologically relevant platform for studying TDP-43 pathology. In the brains of non-human primates and pigs expressing mutant TDP-43(M337V), cytoplasmic mislocalization and aggregate formation closely resemble the pathological features seen in human patient brains (Cohen et al., 2011; Hasegawa et al., 2017; Josephs et al., 2014; McAleese et al., 2017).

To elucidate the neuropathological consequences of cytoplasmic TDP-43 dysfunction, especially its truncated forms, the use of large-animal models that more closely recapitulate human pathology is essential (Li & Lai, 2024). In this study, endogenous TDP-43 was predominantly localized in the nucleus; however, in monkey brains expressing TDP-43(M337V), the absence of nuclear localization signals facilitated the translocation of cleaved TDP-43 fragments onto ribosomes. This process was mediated through interactions with ribosomal large subunit assembly proteins, leading to pronounced neurotoxic effects in the cytoplasm. Ribosome-associated transcriptomic profiling further revealed dysregulation of apoptosis- and lysosome-related genes. These findings demonstrate that truncated TDP-43 associates with ribosomes in the cytoplasm, disrupting the expression of multiple mRNAs involved in apoptosis and lysosomal degradation, ultimately driving neuronal cell death in the primate brain.

## MATERIALS AND METHODS

### Animals and ethics statement

Cynomolgus monkeys were bred at Guangdong Landao Biotechnology Co., Ltd., an institution accredited by the China Association for Assessment and Accreditation of Laboratory Animal Care. All animal-related protocols were approved in advance by the Animal Care and Use Committee of Guangdong Landao Biotechnology Co., Ltd. (approval No. LDACU20201216-02) and Jinan University (approval No. 20210715-18). The company employs dedicated breeders and veterinarians who closely monitor water, temperature, and humidity in the cages, as well as the health of the monkeys. This study was conducted in strict accordance with the "Guidelines for the Care and Use of Laboratory Animals in the Institute of Laboratory Animal Science ($8^{th}$ edition, 2011; National Academies Press)", and adhered to the ARRIVE guidelines for reporting animal research (Kilkenny et al., 2010), ensuring both personnel safety and animal welfare.

### Plasmids, viruses, and antibodies

The cDNAs encoding full-length human TDP-43(M337V) (mutant TDP-43), truncated C-terminal TDP-43-(77-414) (TDP-35(M337V)), or TDP-43-(174-414) (TDP-25(M337V)) were subcloned into adeno-associated virus (AAV) or plasmid enhanced green fluorescent protein (pEGFP) vector (Addgene, 46954 and 10883, USA). The control AAV-EGFP consisted of the same CMV promoter. Primary antibodies included the following: rabbit anti-TDP-43 (1:1 000, Proteintech, 12892-1-AP, USA), rabbit anti-NEUN (1:1 000, Abcam, ab177487, UK), chicken anti-MAP2 (1:5 000, Abcam, 5392, UK), mouse anti-vinculin (1:1 000, Sigma, MAB3574, USA), mouse anti-GAPDH (1:10 000, Proteintech, 60004-1-Ig, USA), rabbit anti-HTRA2 (1:1 000, Proteintech, 15775-1-AP, USA), rabbit anti-BAK1 (1:1 000, CST, 12105S, USA), rabbit anti-BOK (1:1 000, Abcam, ab186745, UK), rabbit anti-CARD6 (1:500, Proteintech, 18029-1-AP, USA), rabbit anti-CTSD (1:1 000, BBI, D264565, China), rabbit anti-CTSZ (1:500, BBI, D220362, China), rabbit anti-CTSC (1:500, BBI, D261516, China), rabbit anti-RPL26 (1:500, Proteintech, 17619-1-AP, USA), and rabbit anti-RPL35 (1:500, Proteintech, 14826-1-AP, USA). All secondary antibodies were purchased from Boster Bio (USA) or Thermo Fisher Scientific (USA).

### Cell culture and transfection

Green monkey kidney fibroblast-like COS7 cell lines were purchased from the American Type Culture Collection (ATCC) and cultured in Dulbecco's Modified Eagle Medium/Nutrient Mixture F-12 (DMEM/F12, 11320033, Invitrogen, USA), containing 10% fetal bovine serum (FBS), 100 U/mL penicillin, 100 μg/mL streptomycin, and 0.25 μg/mL amphotericin B. The cells were maintained at 37°C in 5% $CO_2$ incubators. The growth medium was refreshed every 24 h. For transfection, cells were plated at 70%–80% confluence and transfected with plasmid DNA using Lipofectamine 3000 (Invitrogen, USA) for 24–72 h.

### Surgical procedures

Each monkey was anesthetized by an intraperitoneal injection of 0.3–0.5 mg of atropine, followed by 10–12 mg of ketamine and 15–20 mg of pentobarbital sodium per kg body weight (Li et al., 2021; Underwood & Anthony, 2020). The monkeys were securely positioned on a stereotaxic apparatus (RWD Life Science, China). The precise location of the motor cortex for stereotaxic injection was determined by magnetic resonance imaging (MRI) prior to the procedure. A total of 10 μL of AAV was injected, with AAV-TDP-43, -TDP-35, -TDP-25, and -EGFP titers measured at $10^{13}$ GC/mL, as quantified by the number of packaged vector genomes using quantitative polymerase chain reaction (qPCR). Needle insertion depth was calculated based on pre-surgical MRI data. Eight weeks post-injection, motor cortex tissues from the injected regions were isolated for immunohistochemical and western blot analyses.

### Western blotting and immunofluorescent staining

For western blotting, cultured cells and brain tissues were homogenized in soluble fraction buffer (10 mmol/L Tris, pH 7.4, 100 mmol/L NaCl, 1 mmol/L EDTA, 1 mmol/L EGTA, 0.1% SDS, and 1% Triton X-100) with protease inhibitors (Sigma, P8340, USA). The lysates were diluted in 1× SDS sample buffer and sonicated for 15 s after incubation at 100°C for 10 min. Total lysates (10–20 μg) were loaded in Tris-glycine gel and blotted to a nitrocellulose membrane. The membrane was developed using a Prime Chemiluminescence kit (GE Healthcare Amersham). For immunofluorescent staining, the monkey tissues were perfused with 0.9% NaCl, followed by 4% paraformaldehyde (PFA). Brains were

removed and fixed in 4% PFA overnight at 4°C. The brains were transferred to 30% sucrose for 48 h, then cut into 15-μm sections using a cryostat at −20°C. Sections were blocked in 4% donkey serum with 0.2% Triton X-100 and 3% bovine serum albumin (BSA, Roche Applied Science, BSAV-RO, USA) in 1× phosphate-buffered saline (PBS) for 1 h. The sections were then incubated with primary antibodies in the same buffer at 4°C overnight. After washing with 1× PBS, the sections were incubated with fluorescent secondary antibodies. Fluorescent images were acquired with a Zeiss microscope (Carl Zeiss Imaging, Axiovert 200 MOT, Germany) using either a 40× or 20× lens with a digital camera (Hamamatsu, Orca-100, Japan) and Openlab software (Improvision, UK).

**Subcellular fractionation of brain tissues**

Freshly harvested monkey brain tissues were homogenized using 25 strokes in a Dounce homogenizer with ice-cold buffer (0.32 mol/L sucrose, 15 mmol/L Tris-HCl, 60 mmol/L KCl, 15 mmol/L NaCl, 5 mmol/L EDTA, 1 mmol/L EGTA, 0.02% $NaN_3$, 2 mmol/L ATP, pH 8.0) containing protease inhibitor and 100 μmol/L PMSF. Approximately 10% of the resulting lysates were stored as the total lysate sample. Nuclei and cellular debris were pelleted at 800 ×*g* for 5 min at 4°C. The supernatant was transferred to a new tube and centrifuged at 20 000 ×*g* for 30 min at 4°C, yielding a mitochondrion-enriched pellet. The supernatant was then centrifuged at 100 000 ×*g* for 30 min at 4°C to separate the ribosome-enriched pellet and soluble free-cytoplasmic fraction. Crude nuclear pellets were washed four times with ice-cold homogenization buffer to remove cytoplasmic contaminants. For nuclear purification, the pellets were resuspended in 374 μL of buffer (15 mmol/L HEPES, 1.5 mmol/L $MgCl_2$, 0.2 mmol/L EDTA, 0.5 mmol/L DTT, 26% glycerol, pH 7.9) and mixed with 26 μL of 4.6 mol/L NaCl to generate a final concentration of 300 mmol/L NaCl. The suspension was homogenized with 20 strokes in a homogenizer on ice, then sonicated for 10 s. The homogenized samples were kept on ice for 20 min and centrifuged at 24 000 ×*g* for 20 min at 4°C, then analyzed by western blotting.

**Immunoprecipitation and mass spectrometry**

For immunoprecipitation, 500 μg of brain tissue was lysed in ice-cold 1% NP-40 buffer (50 mmol/L Tris, 50 mmol/L NaCl, 0.1% Triton X-100, 1% NP-40 with 1× protease inhibitors and 100 μmol/L PMSF, pH 7.4). The lysate was precleared using protein A agarose beads (Sigma, P1406, USA), followed by immunoprecipitation with an anti-TDP-43 antibody at 4°C overnight. Protein A agarose beads were added to capture the target proteins, with incubation for 2 h at 4°C. The beads were washed three times in ice-cold lysis buffer, and immunoprecipitated proteins, along with input controls, were subjected to western blotting. For mass spectrometry, the immunoprecipitated proteins were separated by sodium dodecyl-sulfate polyacrylamide gel electrophoresis (SDS-PAGE), and the gel bands were excised and sent to the Beijing Genomics Institute (BGI, China) for protein mass spectrometry analysis.

**RNA sequencing (RNA-seq) and ribosome profiling (RIBO-seq)**

Bulk or ribosome-enriched fractions from the monkey cortex were isolated for transcriptome sequencing. RNA was extracted using TRIzol reagent following the manufacturer's protocols. cDNA library construction and sequencing were performed by Novogene (China). Libraries were sequenced using the Illumina platform, generating 150 bp paired-end reads. Clean reads were obtained using TrimGalore (v.0.6.10) after discarding reads containing adapter sequences, poly-N regions, or low-quality raw data. High-quality reads were aligned to the reference genome from NCBI (https://ftp.ncbi.nlm.nih.gov/genomes/all/GCF/000/364/345/GCF_000364345.1_Macaca_fascicularis_5.0/). More than 30 million read counts were converted from the aligned sequences using HTSeq. Differentially expressed genes (DEGs) were identified based on a fold change>1.3 and an adjusted $P$<0.05.

**RT-qPCR**

Reverse transcription was performed with 1 μg of RNA isolated using the Superscript III First-Strand Synthesis System (Invitrogen, USA). cDNA (1 μL) was combined with 10 μL of SYBR Select Master Mix (Applied Biosystems, USA) and 1 μL of each primer in a 20 μL reaction. The reaction was performed in a real-time thermal cycler (Eppendorf, Realplex Mastercycler, Germany). Relative expression levels were calculated using $2^{-\Delta\Delta CT}$, with AAV-EGFP injection set to 1. The primer sequences were as follows: *BAK1* gene forward: GGGGAACTGTGAATACTTGAA and reverse: CCTATG GGCTCCATCTGC; *BOK* gene forward: CAGCGTCTACC GCAACGT and reverse: CCGCATACAGGGACACCA; *CARD6* gene forward: TGGAGTGTAATGGCACGAT and reverse: AGGCTGAGGCAGGAGAAT; *HTRA2* gene forward: TCCTTTGCCATCCCTTCT and reverse: GGACTCA GGGTCAGCATCA; *BAD* gene forward: TCCTGGTCG GCCATCTTG and reverse: GCCTTCTGCGGCTTCACA; *LAMTOR5* gene forward: GTTCTGGGTCAGGGTGGT and reverse: GGAGGGATTCTTCATTGTG. *CTSB* gene forward: TGGAGACGGCTGTAATGG and reverse: GTGCTCACA GGGAGGGAT; *CTSC* gene forward: GGCTTCCCATACC TCACT and reverse: CCATAGACAACCTCCCACAT; *CTSD* gene forward: CTGGCTCCACCACAAATACA and reverse: CGGTTGATGACGCTGACTT; *CTSH* gene forward: CTGGAG GAAGATAAATGCC and reverse: ATGGAAGGTGGGT AGGGA; *CTSK* gene forward: TTCTGCTGCTACCTGTGA and reverse: GATTTCATCCACCTTGCT; *CTSS* gene forward: TTCATAACCTGGAGCATT and reverse: TCTGATTA GCGTTTGACTT; *CTSZ* gene forward: CTATGCCAG CATCACCCG and reverse: CCAGCGTTAGCACAGTCG. *GAPDH* served as an internal control (forward: ATCTGGC ACCACACCTTCTACA and reverse: TACATGGCTGGGG TGTTGAAGGT).

**Flow cytometry**

Fresh brain tissue was collected and processed to isolate single cells. Samples were first transferred to a tissue culture dish containing 10 mL of 1× PBS. The tissue was minced into 2–4 mm pieces using scissors and subjected to enzymatic digestion using 0.25% trypsin diluted in 1× PBS for 20 min at room temperature. The resulting cell suspension was filtered through a 40 μm nylon mesh strainer to remove clumps and debris. Cells were then centrifuged at 300–500 ×*g* for 4–5 min at 2–8°C, with the supernatant discarded. Single-cell suspensions were fixed and permeabilized using the Cytofix/Cytoperm Solution Kit (BD Biosciences, USA) and stained for 30 min with fluorescein isothiocyanate (FITC)-A and allophycocyanin (APC)-A (BD Biosciences, USA). APC-Annexin V and FITC-Annexin V were used as probes to detect apoptotic cells, binding to negatively charged phospholipid

surfaces with a higher affinity for phosphatidylserine (PS) than other phospholipids. Stained cells were analyzed using a flow cytometer (BD Biosciences, USA) and data were processed with FlowJo software.

**Electron microscopy**

Freshly isolated monkey brain tissue blocks were fixed with 3% glutaraldehyde and 1% osmium tetroxide for 24–48 h. Following multiple rinses with 1× PBS solution, the specimens underwent dehydration using a sequence of acetone concentrations (30%, 50%, 70%, 80%, 90%, 95%, and 100%). The samples were embedded in Eponate 12 (Ted Pella, USA) and ultrathin sections (60 nm) were cut using a Leica Ultracut S ultramicrotome. The sections were placed on copper mesh and stained with uranium acetate at room temperature for 10–15 min, then with lead citrate for 1–2 min. A Hitachi H-7500 electron microscope (Tokyo, Japan) was used for ultrathin section examination.

**Statistical analysis**

Statistical analyses were performed using two-tailed unpaired Student's *t*-tests for pairwise comparisons. One-way analysis of variance (ANOVA) was applied to assess differences among multiple groups, followed by Tukey's *post hoc* test. To account for individual variation among monkeys, data were obtained from three to four independent experiments per group, using tissue samples collected from the same anatomical regions following viral injection. Results are expressed as mean±standard error of the mean (SEM). Statistical calculations were performed using GraphPad Prism, with $P<0.05$ considered statistically significant.

## RESULTS

**Truncated TDP-43 induces neurotoxicity in the monkey brain**

We previously reported that AAV-mediated overexpression of human TDP-43(M337V) in the motor cortex of monkeys leads to cytoplasmic accumulation of exogenous TDP-43 (Yin et al., 2019, 2022). However, the mechanisms by which cytoplasmic TDP-43 contributes to neuropathology remain unclear. To address this, western blotting using a C-terminal-TDP-43 antibody was performed on monkey cortex tissue, revealing abundant truncated TDP-43 fragments (35 and 25 kDa) in mutant TDP-43(M337V)-overexpressing monkeys compared to AAV-EGFP-injected controls (Figure 1A, B). Additionally, an obvious reduction in the mature neuronal markers NEUN and MAP2 was observed, reflecting neuronal toxicity associated with mutant TDP-43 expression (Figure 1B, C).

To further investigate whether cytoplasmic truncated TDP-43 mediates neuropathology, we generated truncated C-terminal TDP-25 or TDP-35 vectors under the same promoter as full-length TDP-43. These constructs were then transfected into cultured monkey COS7 cells (Figure 1D; Supplementary Figure S1). Results showed that truncated TDP-43 fragments were distributed in the cytoplasm, with the smaller TDP-25 fragment exhibiting a greater propensity to form inclusions compared to TDP-35. To assess the in vivo effects, AAV-TDP-35 or AAV-TDP-25 was stereotaxically injected into the right motor cortex of adult monkeys (8–12 years old) (Figure 1E). Two months post-injection, western blot analysis revealed a significant reduction in the neuronal markers NEUN and MAP2 in the injected cortical regions, confirming neuronal loss induced by truncated TDP-43 (35 and 25 kDa) (Figure 1E, F). Immunohistochemical analysis further confirmed extensive neuronal loss in areas proximal to the injection site, where exogenous TDP-35 and TDP-25 expression was most prominent (Figure 2A), compared to the AAV-EGFP-injected controls (Figure 2B, C; Supplementary Figure S2).

**Truncated TDP-43 associates with ribosomes in the monkey brain**

To explore the subcellular distribution of TDP-43 fragments in the cytoplasm, endogenous or full-length TDP-43 was first analyzed in fractions isolated from the injected cortex of wild-type (WT) monkeys. Analysis indicated that TDP-43 was predominantly localized in the nucleus, with minimal presence in ribosomal, mitochondrial, or free-cytoplasmic fractions (Figure 3A, B). However, in the cortex of monkeys expressing mutant (Figure 3C, D) or truncated TDP-43 (Figure 3E, F), a pronounced enrichment of fragmented TDP-43 was observed in ribosome-associated fractions, with some recruitment of full-length TDP-43 in the mitochondrial and free-cytoplasmic fractions. These findings were consistent with observations in TDP-43-transfected monkey COS7 cells, where truncated, but not full-length, TDP-43 exhibited a strong cytoplasmic presence, possibly due to *in vivo* versus *in vitro* differences (Supplementary Figure S3). Immunofluorescence staining further verified the presence of TDP-43 fragments on ribosomes, as indicated by colocalization with ribosomal protein S6 (RPS6) in monkey brain tissue (Supplementary Figure S4).

To explore the molecular mechanism underlying TDP-43 localization to ribosomes, immunoprecipitation of TDP-43 from AAV-TDP-43(M337V)-injected monkey brains was performed (Figure 4A), followed by mass spectrometry to identify interacting proteins. Hierarchical clustering analysis of identified proteins, based on protein abundance and KOG functional classification, revealed significant enrichment of ribosomal large subunit proteins compared to IgG controls (Figure 4B). Specifically, ribosomal protein L26 (RPL26, 22-kDa) and ribosomal protein L35 (RPL35, 15-kDa) were identified as direct TDP-43(M337V) interacting proteins (Figure 4C, D; Supplementary Table S1). Notably, these interactions were absent in endogenous WT TDP-43 (Supplementary Figure S5 and Table S1). Western blot analysis of immunoprecipitated proteins from AAV-TDP-43(M337V)-injected monkey cortices further confirmed that exogenous TDP-43 interacted directly with RPL26 and RPL35 (Figure 4E). Although these findings provide strong evidence of TDP-43-ribosome interactions, direct immunoprecipitation of RPL26 and RPL35 from monkey brain tissue using specific antibodies capable of effectively precipitating monkey RPL26 and RPL35 would further validate these results.

**Truncated TDP-43 disrupts multiple mRNAs in the monkey brain**

The fate of mRNA is influenced by multiple factors, including stability, degradation, and translation efficiency. Ribosome-associated profiling offers a quantitative approach to assess global translation by capturing ribosome-protected RNA fragments, offering deeper insight into translational regulation (Ingolia et al., 2009). Consistent with the mislocalization of TDP-43 to ribosomal fractions, RIBO-seq analysis revealed a greater number of DEGs in the gray matter of the monkey cortex following AAV-mediated expression of mutant TDP-43(M337V). Specifically, 842 genes were up-regulated and 1 008 genes were down-regulated compared to only 223 up-

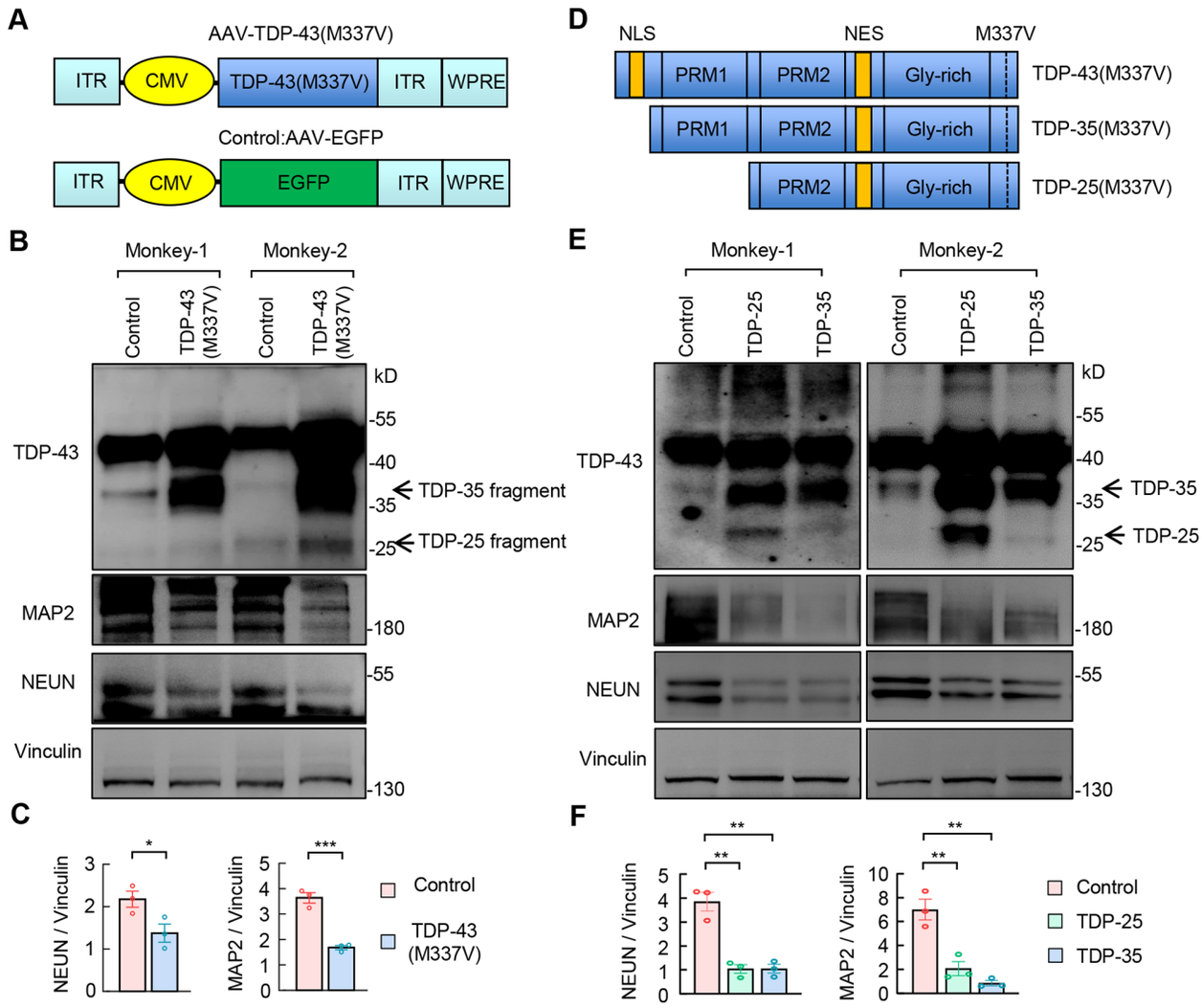


**Figure 1 Expression of mutant and truncated TDP-43 in the monkey brain**

A: Schematic representation of full-length TDP-43(M337V) and EGFP control constructs in AAV vectors under the CMV promoter. B: Western blot analysis of TDP-43(M337V)-overexpressing cortical tissue from 8–12-year-old adult monkeys, 2 months post-injection. TDP-35 and TDP-25 fragments (arrowheads) were detected. Additionally, neuronal markers NEUN and MAP2 were significantly down-regulated in TDP-43(M337V)-expressing monkey tissues compared to AAV-EGFP controls. C: Quantification of NEUN and MAP2 levels, normalized to vinculin, based on western blot analysis. Data represent independent experiments using cortical tissues from AAV-EGFP or AAV-TDP-43(M337V) monkeys ($n$=3 per group). $^{*}$: $P$<0.05; $^{***}$: $P$<0.001. D: Schematic representation of truncated TDP-43(M337V) fragments (35 and 25 kDa), expressed using pEGFP or AAV vectors under the same promoter, for transfection and *in vivo* injection experiments. E: Western blot analysis of truncated mutant TDP-35(M337V) or TDP-25(M337V) (arrowheads, labeled as TDP-35 or TDP-25) in cortical tissue from 8–12-year-old adults, 2 months post-injection, compared to AAV-EGFP controls. NEUN and MAP2 expression was also detected in truncated TDP-35- or TDP-25-expressing monkeys compared to AAV-EGFP controls. F: Quantification of NEUN and MAP2 levels, normalized to vinculin, showing marked reduction following TDP-35 or TDP-25 expression. Data represent independent western blot analyses of AAV-TDP-35- or AAV-TDP-25-injected monkeys ($n$=3 per group). $^{**}$: $P$<0.01.

regulated and 335 down-regulated DEGs identified through bulk RNA-seq (Figure 5A). Additionally, RIBO-seq profiling showed significant changes in the percentage of reads mapped to different genomic regions in the AAV-TDP-43(M337V) injected monkey cortex compared to the AAV-EGFP controls (Figure 5B).

KEGG pathway analysis (http://kobas.cbi.pku.edu.cn/genelist/) further highlighted significant enrichment in pathways associated with “apoptosis progression” and “lysosome decay” in the AAV-TDP-43(M337V)-injected monkeys compared to the AAV-EGFP controls (Figure 5C). Notably, several apoptosis- and lysosome-related genes exhibited significant translational alterations in RIBO-seq data, which were not reflected in the bulk RNA-seq (Figure 5D). For example, pro-apoptotic genes such as *BAK1* and *HTRA2* were markedly up-regulated in the AAV-TDP-43(M337V)-injected monkey cortex, while apoptosis-suppressing genes such as *CARD6*, *CTSC*, *CTSD*, and *CTSZ*, which encode key cathepsin proteases involved in lysosomal function, were markedly downregulated in RIBO-seq profiling. To validate these findings, RT-qPCR was performed, confirming that DEGs associated with apoptosis progression and lysosome degradation were consistent with the RIBO-seq data RT-qPCR(Figure 5E), while no significant changes were detected at the bulk RNA level (Supplementary Figure S6).

**Truncated TDP-43 induces apoptosis and lysosomal dysfunction**

To determine whether downstream apoptosis- and lysosome-

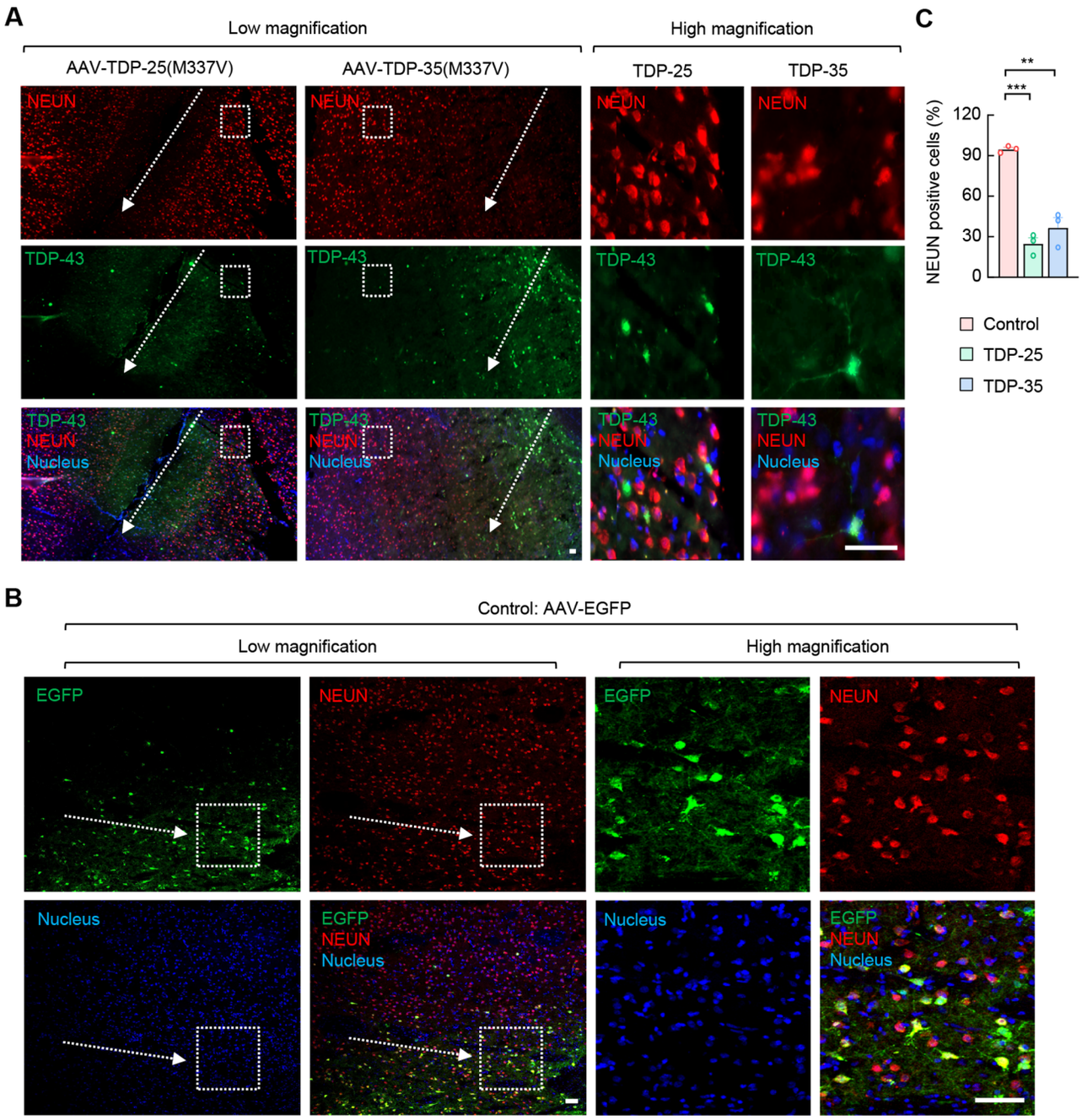


**Figure 2 Truncated TDP-43 induces neurotoxicity in the monkey brain**

A: Immunofluorescence double-staining of TDP-43 and NEUN, revealing a marked reduction in NEUN expression in the monkey cortex following TDP-35 and TDP-25 expression, compared to uninjected brain regions. Dotted line with arrowheads indicates injection pathway. Right panels show higher-magnification images of immunofluorescent staining in the white-dotted box from the left panel (low magnification). Cytoplasmic distribution of truncated TDP-35 and TDP-25 was observed. Scale bar: 40 μm. B: Immunofluorescence staining of NEUN, showing AAV-EGFP expression had no detectable effect on NEUN levels in the monkey cortex compared with the uninfected brain regions. Dotted line with arrowheads indicates injection pathway. Right panels show higher-magnification images of immunofluorescent staining in the white-dotted box from the left panel (low magnification). Scale bar: 40 μm. C: Quantification of NEUN-positive cells in exogenous TDP-25-, TDP-35-, and EGFP-expressing cells. Data represent three independent experiments using infected tissues from AAV-TDP-25-, AAV-TDP-35-, or AAV-EGFP-expressing monkeys ($n$=3 per group). $^{**}$: $P$<0.01; $^{***}$: $P$<0.001.

related genes contribute to the neurotoxicity of truncated TDP-43, we examined key apoptosis-promoting proteins (BAK1, BOK, and HTRA2), apoptosis-suppressing proteins (CARD6, CTSC, CTSD, and CTSZ), and cathepsin protease family members (CTSC, CTSD, and CTSZ) in AAV-TDP-43(M337V)-injected monkey cortices by western blotting (Figure 6A, B). Next, single-cell suspensions were isolated from monkey brains and analyzed using flow cytometry. The percentage of FITC-A-positive cells, representing total apoptotic cells, was significantly higher in TDP-25(M337V) and TDP-35(M337V)-expressing monkey brains compared to AAV-EGFP controls (Figure 6C, D). To further assess lysosomal alterations, we performed electron microscopy (EM). In the AAV-EGFP-injected control cortex, dense lysosomes were predominantly

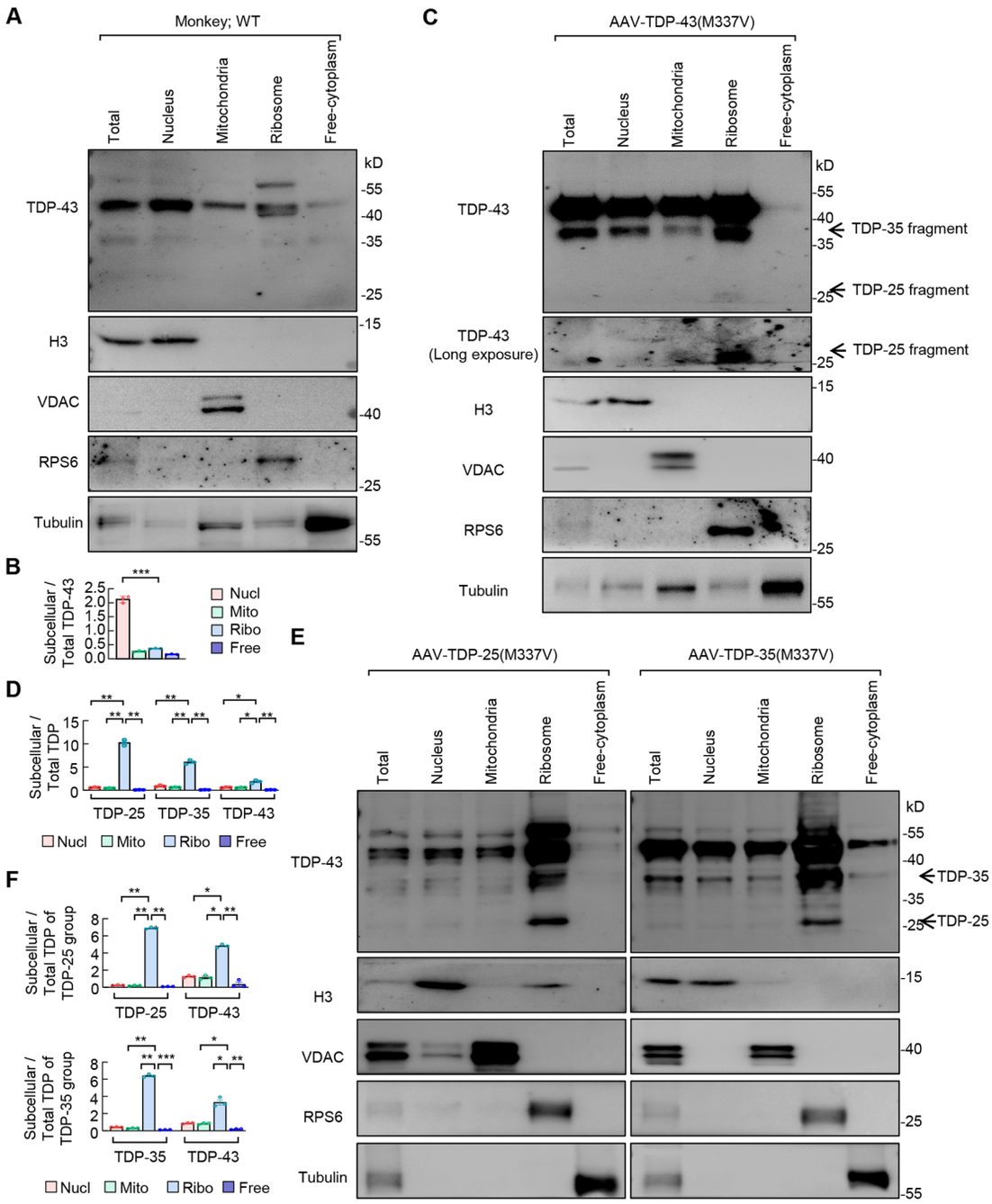


**Figure 3 Mutant and truncated TDP-43 localizes to ribosomes in the monkey brain**

A: Subcellular distribution of endogenous TDP-43 in wild-type (WT) monkey brains (8–12 years old), examined by sucrose density gradient centrifugation. Brain tissues were fractioned for subcellular localization using H3, VDAC, RPS6, and tubulin antibodies as nuclear, mitochondrial, ribosomal, and free-cytoplasmic markers, respectively. B: Quantitative analysis of western blot analysis, showing high nuclear localization of endogenous TDP-43 in WT monkey brains, with significantly lower abundance in ribosomal, mitochondrial, and free-cytoplasmic fractions. Data represent mean±SEM from three independent experiments, ***: $P$<0.001. C: Subcellular localization of mutant TDP-43 (TDP-43(M337V)) in monkey brains (8–12 years old) was analyzed by sucrose density centrifugation. Fractioned brain tissues were examined using H3, VDAC, RPS6, and tubulin antibodies as nuclear, mitochondrial, ribosomal, and free-cytoplasmic markers, respectively. Western blotting showed that cytoplasmic TDP-43 fragments (TDP-35 and TDP-25) predominantly localized to ribosomes, where they exhibited aggregation and recruitment of full-length TDP-43. D: Quantification of subcellular distribution of TDP-25 and TDP-35 fragments in AAV-TDP-43(M337V)-expressing monkey brains. Ribosome-associated TDP-43 fragments were significantly enriched compared to mitochondrial and free-cytoplasmic fractions. Data represent mean±SEM from three independent experiments, *: $P$<0.05; **: $P$<0.01. E: Subcellular localization of AAV-TDP-25 or AAV-TDP-35 expression in monkey brains (8–12 years old) was assessed using sucrose density centrifugation. Fractioned brain tissues were examined using H3, VDAC, RPS6, and tubulin antibodies. Western blotting confirmed that truncated TDP-35 and TDP-25 were mainly localized to ribosomal fractions. F: Quantification of subcellular distribution of truncated TDP-25 and TDP-35, as well as recruited full-length TDP-43, in the monkey brain. Cytoplasmic fractions exhibited the highest accumulation of TDP-25 and TDP-35 in the ribosome compared to mitochondrial and free-cytoplasmic fractions. Data represent mean±SEM from three independent experiments, *: $P$<0.05; **: $P$<0.01; ***: $P$<0.001.

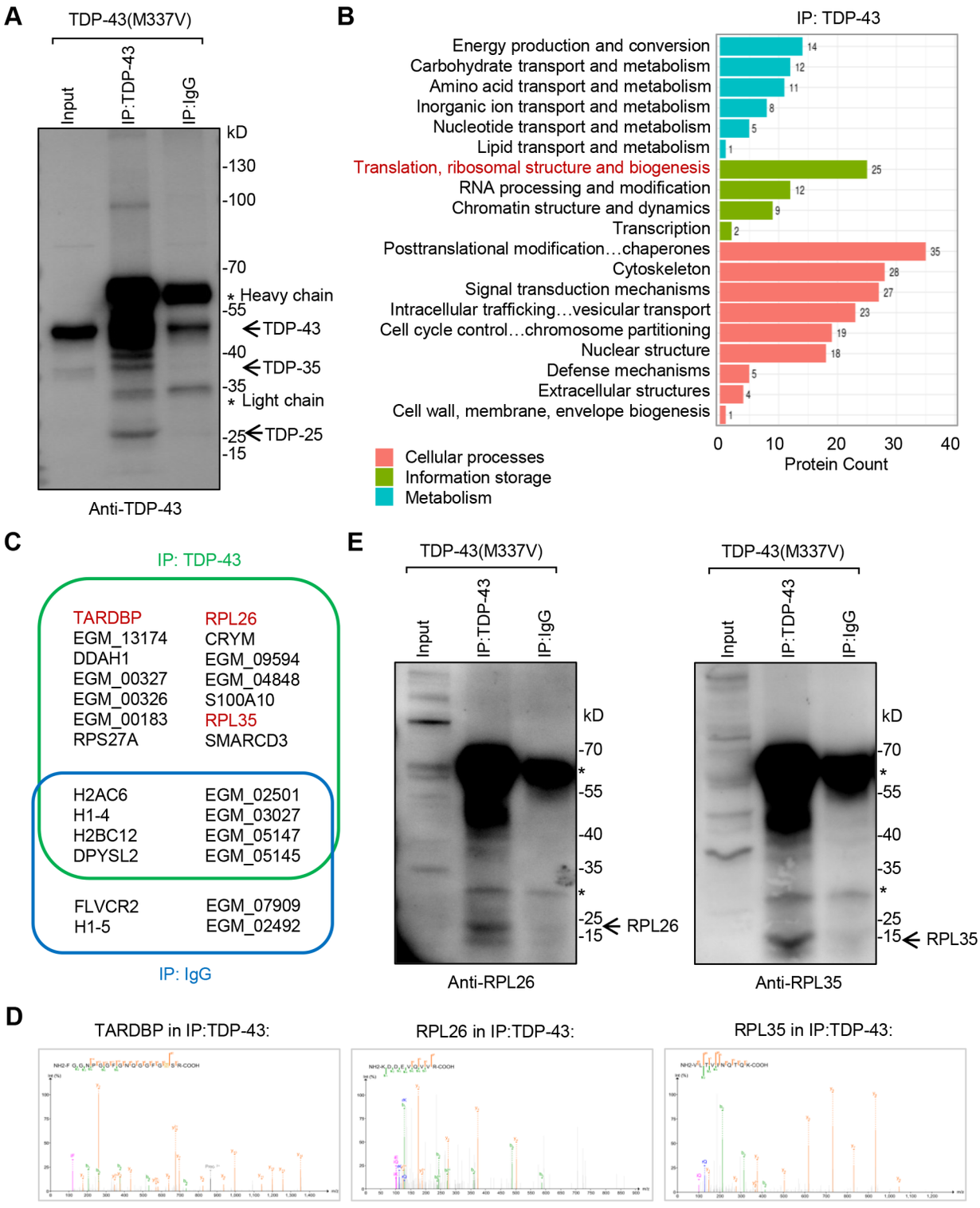


**Figure 4 Pathological TDP-43 interacts with ribosomal large subunit assembly proteins**

A: Western blot analysis of immunoprecipitated TDP-43 and truncated fragments (arrows) from AAV-TDP-43(M337V)-injected monkey cortex, used for proteomic sequencing. B: Mass spectrometry analysis and hierarchical clustering of TDP-43-interacting compared to IgG immunoprecipitation controls. “Protein count” represents enriched biological clusters, with proteins categorized by function, including those involved in “Translation, ribosomal structure and biogenesis”. C: List of interacting proteins identified in proteomic analysis. Green cycles indicate proteins identified in the immunoprecipitated TDP-43 complex, blue cycles represent proteins in the IgG group. RPL26 and RPL35 were specifically enriched in the TDP-43 complex, but not in the IgG control. D: Mass spectrometry analysis of immunoprecipitated TDP-43, highlighting enriched signals in the precipitated TDP-43 complex from monkey cortical tissue. Amino acid sequences of TDP-43 (TARDBP), RPL26 and RPL35 were detected, indicating their presence in the precipitated complex. E: Western blot analysis of AAV-TDP-43(M337V)-injected monkey cortex showed that exogenous mutant TDP-43 associates with ribosomal large subunit assembly components RPL26 (22 kDa) and RPL35 (15 kDa) (arrows). IgG precipitation served as a control.

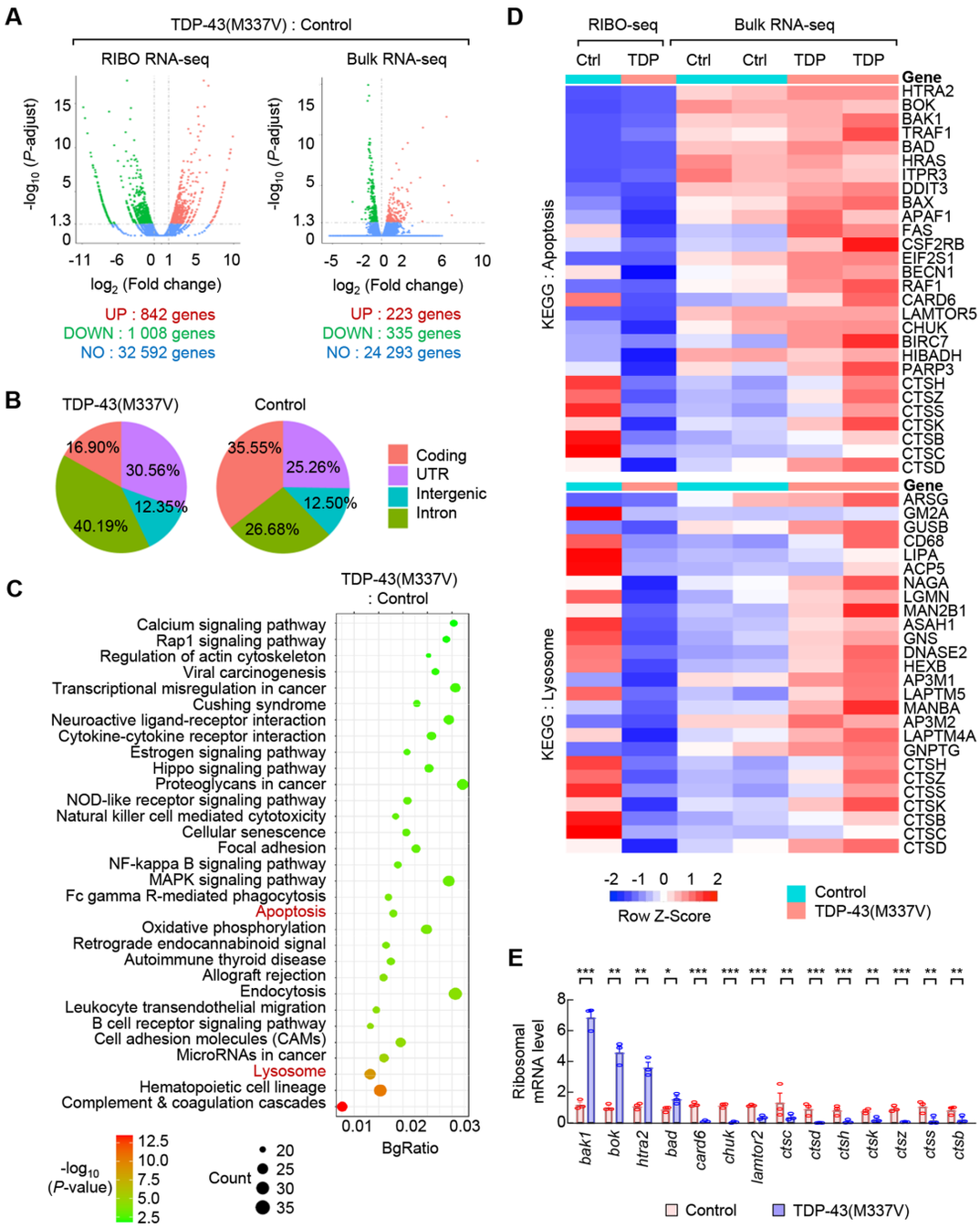


**Figure 5 Pathological TDP-43 alters multiple mRNAs in the monkey brain**

A: Volcano plot analysis of RIBO-seq analysis, revealing a greater number of differentially expressed genes (DEGs) in the cortical gray matter of monkeys expressing AAV-TDP-43(M337V) compared to AAV-EGFP controls. Specifically, 842 genes were up-regulated (red) and 1 008 genes were down-regulated (green), whereas only 223 up-regulated and 335 down-regulated DEGs were present in the same tissues based on bulk RNA-seq. B: RIBO-seq profiling showing changes in the distribution of mapped reads across genomic regions, including coding (16.90%) and intron fragments (40.19%) in the gray matter of AAV-TDP-43(M337V) monkeys compared to coding (35.55%) and intron fragments (26.68%) in AAV-EGFP controls. C: KEGG pathway analysis showing significant enrichment in pathways associated with apoptosis and lysosomal function in the RIBO-seq dataset from AAV-TDP-43(M337V)-expressing monkey cortex compared to AAV-EGFP controls. D: Heatmap analysis of key apoptosis- and lysosome-related genes in the RIBO-seq dataset from AAV-TDP-43(M337V)-expressing monkey cortex, showing changes in apoptosis-promoting genes *BAK1*, *BOK*, *HTRA2*, *BAD*, apoptosis-suppressing genes *CARD6*, *CHUK*, and *LAMTOR5*, and cathepsin proteases family members *CTSC*, *CTSD*, *CTSK*, *CTSH*, *CTSZ*, *CTSS*, and *CTSD*. Notably, these DEGs were not significantly altered in the bulk RNA-seq data from the same tissue. E: RT-qPCR verification of ribosome-associated gene dysregulation in AAV-TDP-43(M337V)-injected monkey cortex. Apoptosis-promoting genes *BAK1*, *BOK*, *HTRA2*, and *BAD* were up-regulated, while apoptosis-suppressing genes *CARD6*, *CHUK*, and *LAMTOR5* were down-regulated in AAV-TDP-43(M337V)-injected monkey cortex compared to AAV-EGFP controls. Apoptosis progression and lysosomal-decay co-associated genes *CTSC*, *CTSD*, *CTSK*, *CTSH*, *CTSZ*, *CTSS*, and *CTSD* were also down-regulated following TDP-43(M337V) expression. RT-qPCR data were analyzed using the $2^{-\Delta\Delta Ct}$ method, and relative transcript levels of each gene were normalized to GAPDH. Data represent mean±SEM from three independent experiments, $^{*}$: $P$<0.05; $^{**}$: $P$<0.01; $^{***}$: $P$<0.001.

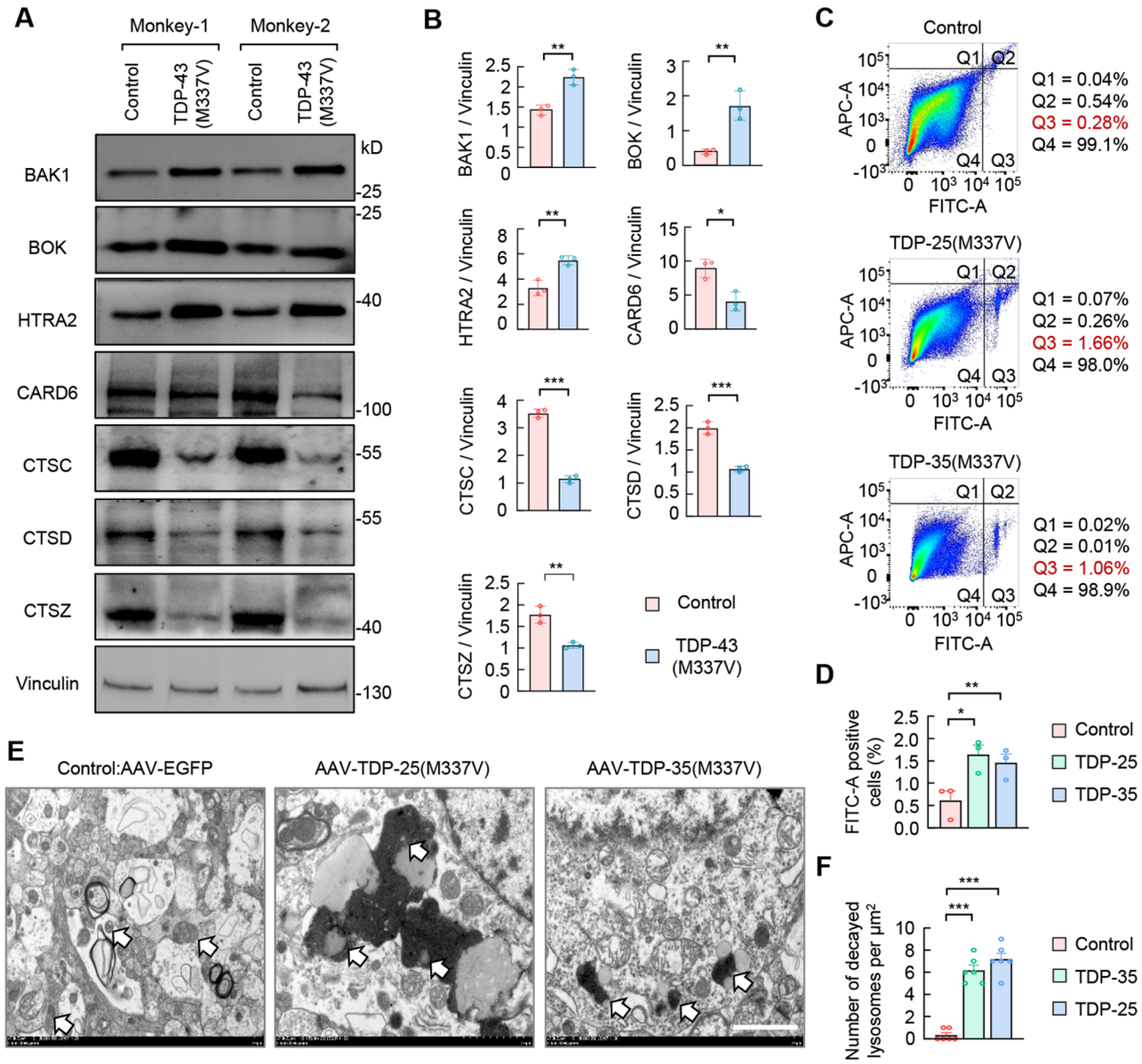


**Figure 6 Truncated TDP-43 induces apoptosis and lysosomal decay in the monkey brain**

A: Western blot analysis of apoptosis- and lysosome-related proteins in TDP-43(M337V)-expressing monkey cortex. Apoptosis-promoting proteins BAK1, BOK, and HTRA2 increased, while apoptosis-suppressing proteins CARD6, CTSC, CTSD, and CTSZ decreased, with the breakdown of cathepsin family members CTSC, CTSD, and CTSZ indicating lysosomal degradation compared to EGFP controls. B: Quantification of apoptosis- and lysosome-related protein levels, including BAK1, BOK, HTRA2, CARD6, CTSC, CTSD, and CTSZ, normalized to vinculin, in TDP-43(M337V)-expressing monkey brain. Data represent mean±SEM from three independent experiments, $^{*}$: $P$<0.05; $^{**}$: $P$<0.01; $^{***}$: $P$<0.001. C: Flow cytometry analysis of apoptosis in truncated TDP-35(M337V)- or TDP-25(M337V)-expressing monkey cortex compared to EGFP controls. Single-cell suspensions were stained and analyzed, showing a higher percentage of FITC-A-positive apoptotic cells compared to controls. D: Quantification of FITC-A-positive cells in exogenous TDP-25-, TDP-35-, or EGFP-expressing tissues. TDP-25- and TDP-35-expressing monkeys exhibited significantly higher apoptotic cell numbers compared to EGFP controls. Data represent three independent experiments from AAV-TDP-25(M337V)-, AAV-TDP-35(M337V)-, or AAV-EGFP-expressing monkeys ($n$=3 per group). $^{*}$: $P$<0.05; $^{**}$: $P$<0.01. E: Representative electron microscopy (EM) images of truncated AAV-TDP-25(M337V)- or AAV-TDP-35(M337V)-injected monkey cortex, showing lysosomal impairment compared to AAV-EGFP controls. Arrowheads indicate intact lysosomes in EGFP-expressing tissue, while truncated TDP-43 expression led to lysosomal decay, swelling, and fusion of double-membrane structures containing undigested residues. Scale bars: 2 μm. F: Quantification of decayed lysosomes per μm$^2$ in TDP-25-, TDP-35-, or EGFP-expressing monkey cortex. TDP-25 and TDP-35 expression significantly increased lysosomal decay compared to EGFP controls. Data were obtained from 10 random images across three independent experiments from AAV-TDP-25(M337V), AAV-TDP-35(M337V), or AAV-EGFP injected monkeys ($n$=3 per group). $^{***}$: $P$<0.001.

localized in the perikaryon of neurons containing paired helical filaments. In contrast, neurons expressing mutant truncated TDP-43 exhibited displaced, yet morphologically normal-appearing nuclei, scattered bundles of paired helical filaments, numerous dense autophagic vacuoles, lipofuscin granules, and small dense lysosomes, indicating lysosomal dysfunction and progressive neurodegeneration (Figure 6E, F).

In summary, in primate neurons, exogenous mutant or

truncated TDP-43 becomes mislocalized to ribosomes, where it interacts with ribosomal large subunit assembly proteins RPL26 and RPL35, ultimately triggering neuronal cell death. Ribosome profiling also revealed that pathological TDP-43 dysregulates certain genes associated with apoptosis progression and lysosomal degradation, contributing to its neurotoxic gain-of-function.

## DISCUSSION

Cytoplasmic TDP-43 aggregates are present in the brains and spinal cords of 97% of ALS cases and 45% of FTLD cases (Arai et al., 2006; Chen-Plotkin et al., 2010; Janssens & Van Broeckhoven, 2013; Neumann et al., 2006; Prpar Mihevc et al., 2017), with additional involvement in other neurological disorders, including 57% of AD cases and some LBD cases (Colom-Cadena et al., 2017; Hasegawa et al., 2017; Josephs et al., 2014; McAleese et al., 2017; Ticozzi et al., 2011). The mislocalization of TDP-43 in the cytoplasm can result in a corresponding loss of its nuclear function, disrupting RNA metabolism and protein homeostasis in affected neurons (Arai et al., 2006; Geser et al., 2010; Neumann et al., 2006). Interestingly, TDP-43 mutations are found in fewer than 5% of ALS patients (Cohen et al., 2011; Kabashi et al., 2008; Lagier-Tourenne & Cleveland, 2009; Renton et al., 2014), suggesting that cytoplasmic accumulation of TDP-43 occurs independently of genetic mutations and is likely influenced by species-specific regulatory mechanisms. For example, transgenic rodent models overexpressing WT or mutant TDP-43 predominantly exhibit nuclear localization of the protein (Gendron et al., 2013; Huang et al., 2012; Shan et al., 2010; Swarup et al., 2011; Watanabe et al., 2020; Wegorzewska et al., 2009). In contrast, mutant TDP-43 expression in the brains and spinal cords of monkeys results in cytoplasmic distribution, mirroring the pathological features observed in human ALS and FTLD (Jackson et al., 2015; Uchida et al., 2012; Yin et al., 2019). Similarly, TDP-43-expressing transgenic pigs exhibit cytoplasmic accumulation of exogenous TDP-43 (Wang et al., 2015). A key factor driving primate-specific TDP-43 cytoplasmic accumulation is the action of caspase-4, which is selectively expressed in primate brains and cleaves TDP-43, removing its N-terminal nuclear import signals, thereby facilitating cytoplasmic accumulation of C-terminal fragments (Li et al., 2015; Yin et al., 2019). These truncated TDP-43 fragments closely resemble those observed in patient brains (Cohen et al., 2011; Hasegawa et al., 2017; Josephs et al., 2014; McAleese et al., 2017). Given these findings, the non-human primate models provide a physiologically relevant platform to investigate the pathological consequences of cytoplasmic TDP-43 dysfunction and its contribution to neurodegeneration. Furthermore, the use of large-animal models with greater phylogenetic proximity to humans is essential for systematically evaluating interspecies conservation of the pathogenesis of TDP-43.

As an RNA-binding protein, TDP-43 primarily exists in the nucleus, where it regulates gene transcription and alternative splicing of transcribed pre-mRNA (Gendron et al., 2013; Philips & Rothstein, 2015; Ratti & Buratti, 2016). Its nucleic acid-binding activity is mediated by two conserved RNA recognition motifs (RRM1 and RRM2) (Buratti et al., 2005; Prakash et al., 2021). Additionally, a C-terminal glycine-rich domain (aa 277-414)—which is retained in TDP-25 and TDP-35—facilitates interactions with a broad range of proteins (D' Ambrogio et al., 2009; Freibaum et al., 2010; Kitamura et al., 2024; Lagier-Tourenne & Cleveland, 2009; Pesiridis et al., 2009). This domain is also likely involved in ribosome binding, thereby altering gene translation. Supporting this hypothesis, TDP-43 overexpression, including ALS-linked mutants, has been detected in axons, where it disrupts mRNA transport of key neuronal transcripts such as NF-L, PSD-95, CaMKIIα, and MAP1B (Alami et al., 2014; Coyne et al., 2014; Fallini et al., 2012; Ishiguro et al., 2016). These transported functional mRNAs undergo local translation on ribosomes, allowing neurons to rapidly respond to stimuli or injury by modulating axon elongation and synapse formation (Kelleher III et al., 2004). For instance, TDP-43 collaborates with fragile X mental retardation protein (FMRP) to regulate Rac1 mRNA translation in neuronal dendrites (Chu et al., 2019; Majumder et al., 2016). Despite accumulating evidence implicating mislocalized TDP-43 in neuropathology, most studies have focused on full-length or non-fragmented TDP-43 in cultured cells or small-animal models, leaving the pathogenic role of cytoplasmic truncated TDP-43 poorly understood. Notably, CTF-25 transgenic mice generated using the CaMKIIa promoter (forebrain-specific expression) or NEFH and PrP promoters (targeting the brain and spinal cord) exhibit no overt motor or cognitive deficits (Spiller et al., 2018; Tsuiji et al., 2017; Walker et al., 2015). Similarly, transgenic mice subjected to Thy1.2-driven neuronal expression do not display any significant motor dysfunction or neurodegeneration at 2 or 6 months of age, although some memory impairments emerge under specific conditions such as aging and stress hormone modulation (Caccamo et al., 2012, 2013, 2015). In *Drosophila* models, transgenic expression of full-length TDP-43 or ALS-linked mutations results in a shortened lifespan (Voigt et al., 2010) and exacerbates age-dependent motor decline (Li et al., 2010), effects that are notably more severe than those induced by TDP-43 CTFs. The absence of hallmark TDP-43 proteinopathy features following TDP-43 CTF expression in small animals suggests that rather than being a central driver of disease, CTFs may be by-product or consequence of mechanisms that do not directly cause neurodegeneration across multiple model organisms.

This study explored the effects of cytoplasmic TDP-43 in neuronal dysfunction, revealing its ability to dysregulate apoptosis- and lysosome-associated RNAs under pathological conditions. Our findings suggest that nuclear and cytoplasmic TDP-43 differentially regulate mRNAs processing and translation, underscoring distinct functional consequences of its mislocalization. Using a non-human primate model, we found that endogenous WT TDP-43 was primarily localized in the nucleus under physiological conditions. However, TDP-35 and TDP-25 fragments, lacking the nuclear localization signal, accumulated in the cytoplasm, where they associated with ribosomes and formed aggregates. Notably, previous studies have reported that C-terminal fragments (30–35 kDa) can sequester endogenous nuclear TDP-43, leading to its depletion in ALS and FTLD patient brains (Che et al., 2011, 2012, 2015; Nishimoto et al., 2010; Nonaka et al., 2009). To investigate the functional consequences of this ribosome-associated TDP-43 pathology, we conducted ribosome profiling, which identified widespread dysregulation of apoptosis and lysosome-related genes. These findings align with previous reports demonstrating that mislocalized TDP-43 disrupts translational machinery in cultured cells and small-animal models. For instance, in rodent motor neuron-like cells and primary cultured neurons, human mutant TDP-43

overexpression has been shown to enhance the translation of specific mRNAs (Neelagandan et al., 2019). Additionally, cytoplasmic TDP-43 disrupts global protein synthesis (Russo et al., 2017), and alters ribosome-associated mRNA expression, as seen with glypican Dally-like protein/GPC6 (Lehmkuhl et al., 2021). TDP-43(M337V) knock-in mice, despite exhibiting splicing deregulation, do not show neurodegeneration, as nuclear TDP-43(M337V) remains predominant in the absence of cytoplasmic TDP-43 cleavage (Watanabe et al., 2020).

A key insight from our non-human primate model is that cytoplasmic TDP-43 associates with ribosomes and modulates the translation of multiple mRNAs, implicating ribosome-bound TDP-43 as a critical driver of neurotoxicity. However, the pathogenic effects of cytoplasmic TDP-43 may be context-dependent, influenced by specific fragment types and species-specific differences. Furthermore, whether the dysregulation of apoptosis- and lysosome-related genes arises primarily from ribosomal translation defects or secondarily from broader cellular dysfunction remains an open question, warranting further investigation.

## DATA AVAILABILITY

All sequencing datasets were deposited into the Science Data Bank (DOI: 10.57760/sciencedb.j00139.00142), Genome Sequence Archive (GSA, accession No. CRA021067), and National Center for Biotechnology Information (NCBI, BioProjectID PRJNA1195234) databases.

## SUPPLEMENTARY DATA

Supplementary data to this article can be found online.

## COMPETING INTERESTS

The authors declare that they have no competing interests.

## AUTHORS' CONTRIBUTIONS

P.Y. and X.J.L. designed the research. F.Y.D., G.L.Z., K.L.O., L.H.Z., Q.Q.J., X.W., and M.W.G. performed the research and analyzed the data. B.L. assisted with monkey maintenance and surgery. S.H.L. provided technical guidance. P.Y. and X.J.L. wrote the paper. All authors read and approved the final version of the manuscript.

## ACKNOWLEDGMENTS

The authors thank all members of Li Laboratory for helpful discussions, as well as the staff at Jinan University and Guangdong Landao Co. Ltd. for assistance with animal care and experiments.

## REFERENCES

Alami NH, Smith RB, Carrasco MA, et al. 2014. Axonal transport of TDP-43 mRNA granules is impaired by ALS-causing mutations. *Neuron*, **81**(3): 536–543.

Arai T, Hasegawa M, Akiyama H, et al. 2006. TDP-43 is a component of ubiquitin-positive tau-negative inclusions in frontotemporal lobar degeneration and amyotrophic lateral sclerosis. *Biochemical and Biophysical Research Communications*, **351**(3): 602–611.

Broeck LV, Callaerts P, Dermaut B. 2014. TDP-43-mediated neurodegeneration: towards a loss-of-function hypothesis?. *Trends in Molecular Medicine*, **20**(2): 66–71.

Buratti E. 2015. Functional significance of TDP-43 mutations in disease. *Advances in Genetics*, **91**: 1–53.

Buratti E, Brindisi A, Giombi M, et al. 2005. TDP-43 binds heterogeneous nuclear ribonucleoprotein A/B through its C-terminal tail: an important region for the inhibition of cystic fibrosis transmembrane conductance regulator exon 9 splicing. *Journal of Biological Chemistry*, **280**(45): 37572–37584.

Caccamo A, Majumder S, Oddo S. 2012. Cognitive decline typical of frontotemporal lobar degeneration in transgenic mice expressing the 25-kDa C-terminal fragment of TDP-43. *The American Journal of Pathology*, **180**(1): 293–302.

Caccamo A, Medina DX, Oddo S. 2013. Glucocorticoids exacerbate cognitive deficits in TDP-25 transgenic mice via a glutathione-mediated mechanism: implications for aging, stress and TDP-43 proteinopathies. *Journal of Neuroscience*, **33**(3): 906–913.

Caccamo A, Shaw DM, Guarino F, et al. 2015. Reduced protein turnover mediates functional deficits in transgenic mice expressing the 25 kDa C-terminal fragment of TDP-43. *Human Molecular Genetics*, **24**(16): 4625–4635.

Che MX, Jiang LL, Li HY, et al. 2015. TDP-35 sequesters TDP-43 into cytoplasmic inclusions through binding with RNA. *FEBS Letters*, **589**(15): 1920–1928.

Che MX, Jiang LL, Zhou CJ, et al. 2012. Aggregation of TDP-43 fragments triggers cellular aberrant function: implication in neurodegeneration. *Molecular Neurodegeneration*, **7**: O1.

Che MX, Jiang YJ, Xie YY, et al. 2011. Aggregation of the 35‐kDa fragment of TDP‐43 causes formation of cytoplasmic inclusions and alteration of RNA processing. *The FASEB Journal*, **25**(7): 2344–2353.

Chen-Plotkin AS, Lee VMY, Trojanowski JQ. 2010. TAR DNA-binding protein 43 in neurodegenerative disease. *Nature Reviews Neurology*, **6**(4): 211–220.

Chu JF, Majumder P, Chatterjee B, et al. 2019. TDP-43 regulates coupled dendritic mRNA transport-translation processes in co-operation with FMRP and Staufen1. *Cell Reports*, **29**(10): 3118–3133. e6.

Cohen TJ, Lee VMY, Trojanowski JQ. 2011. TDP-43 functions and pathogenic mechanisms implicated in TDP-43 proteinopathies. *Trends in Molecular Medicine*, **17**(11): 659–667.

Colom-Cadena M, Grau-Rivera O, Planellas L, et al. 2017. Regional overlap of pathologies in Lewy body disorders. *Journal of Neuropathology & Experimental Neurology*, **76**(3): 216–224.

Coyne AN, Siddegowda BB, Estes PS, et al. 2014. Futsch/MAP1B mRNA is a translational target of TDP-43 and is neuroprotective in a *Drosophila* model of amyotrophic lateral sclerosis. *Journal of Neuroscience*, **34**(48): 15962–15974.

D'Ambrogio A, Buratti E, Stuani C, et al. 2009. Functional mapping of the interaction between TDP-43 and hnRNP A2 *in vivo*. *Nucleic Acids Research*, **37**(12): 4116–4126.

Dayton RD, Gitcho MA, Orchard EA, et al. 2013. Selective forelimb impairment in rats expressing a pathological TDP-43 25 kDa C-terminal fragment to mimic amyotrophic lateral sclerosis. *Molecular Therapy*, **21**(7): 1324–1334.

Fallini C, Bassell GJ, Rossoll W. 2012. The ALS disease protein TDP-43 is actively transported in motor neuron axons and regulates axon outgrowth. *Human Molecular Genetics*, **21**(16): 3703–3718.

Freibaum BD, Chitta RK, High AA, et al. 2010. Global analysis of TDP-43 interacting proteins reveals strong association with RNA splicing and translation machinery. *Journal of Proteome Research*, **9**(2): 1104–1120.

Gendron TF, Rademakers R, Petrucelli L. 2013. *TARDBP* mutation analysis in TDP-43 proteinopathies and deciphering the toxicity of mutant TDP-43. *Journal of Alzheimer's Disease*, **33**(S1): S35–S45.

Geser F, Lee VMY, Trojanowski JQ. 2010. Amyotrophic lateral sclerosis and frontotemporal lobar degeneration: a spectrum of TDP‐43 proteinopathies. *Neuropathology*, **30**(2): 103–112.

Gregory JM, Barros TP, Meehan S, et al. 2012. The aggregation and neurotoxicity of TDP-43 and its ALS-associated 25 kDa fragment are differentially affected by molecular chaperones in *Drosophila*. *PLoS One*, **7**(2): e31899.

Guo L, Shorter J. 2017. Biology and pathobiology of TDP-43 and emergent therapeutic strategies. *Cold Spring Harbor Perspectives in Medicine*, **7**(9): a024554.

Hasegawa M, Nonaka T, Masuda-Suzukake M. 2017. Prion-like mechanisms and potential therapeutic targets in neurodegenerative disorders. *Pharmacology & Therapeutics*, **172**: 22–33.

Huang C, Tong JB, Bi FF, et al. 2012. Mutant TDP-43 in motor neurons promotes the onset and progression of ALS in rats. *The Journal of Clinical Investigation*, **122**(1): 107–118.

Ingolia NT, Ghaemmaghami S, Newman JRS, et al. 2009. Genome-wide analysis in vivo of translation with nucleotide resolution using ribosome profiling. *Science*, **324**(5924): 218–223.

Ishiguro A, Kimura N, Watanabe Y, et al. 2016. TDP‐43 binds and transports G‐quadruplex‐containing mRNAs into neurites for local translation. *Genes to Cells*, **21**(5): 466–481.

Jackson KL, Dayton RD, Fisher‐Perkins JM, et al. 2015. Initial gene vector dosing for studying symptomatology of amyotrophic lateral sclerosis in non‐human primates. *Journal of Medical Primatology*, **44**(2): 66–75.

Janssens J, Van Broeckhoven C. 2013. Pathological mechanisms underlying TDP-43 driven neurodegeneration in FTLD–ALS spectrum disorders. *Human Molecular Genetics*, **22**(R1): R77–R87.

Janssens J, Wils H, Kleinberger G, et al. 2013. Overexpression of ALS-associated p. M337V human TDP-43 in mice worsens disease features compared to wild-type human TDP-43 mice. *Molecular Neurobiology*, **48**(1): 22–35.

Josephs KA, Whitwell JL, Weigand SD, et al. 2014. TDP-43 is a key player in the clinical features associated with Alzheimer's disease. *Acta Neuropathologica*, **127**(6): 811–824.

Kabashi E, Lin L, Tradewell ML, et al. 2010. Gain and loss of function of ALS-related mutations of *TARDBP* (TDP-43) cause motor deficits *in vivo*. *Human Molecular Genetics*, **19**(4): 671–683.

Kabashi E, Valdmanis PN, Dion P, et al. 2008. *TARDBP* mutations in individuals with sporadic and familial amyotrophic lateral sclerosis. *Nature Genetics*, **40**(5): 572–574.

Kelleher III RJ, Govindarajan A, Tonegawa S. 2004. Translational regulatory mechanisms in persistent forms of synaptic plasticity. *Neuron*, **44**(1): 59–73.

Kilkenny C, Browne WJ, Cuthill IC, et al. 2010. Improving bioscience research reporting: the ARRIVE guidelines for reporting animal research. *Journal of Pharmacology and Pharmacotherapeutics*, **1**(2): 94–99.

Kitamura A, Fujimoto A, Kawashima R, et al. 2024. Hetero-oligomerization of TDP-43 carboxy-terminal fragments with cellular proteins contributes to proteotoxicity. *Communications Biology*, **7**(1): 743.

Kwong LK, Neumann M, Sampathu DM, et al. 2007. TDP-43 proteinopathy: the neuropathology underlying major forms of sporadic and familial frontotemporal lobar degeneration and motor neuron disease. *Acta Neuropathologica*, **114**(1): 63–70.

Lagier-Tourenne C, Cleveland DW. 2009. Rethinking ALS: the fus about TDP-43. *Cell*, **136**(6): 1001–1004.

Lee EB, Lee VMY, Trojanowski JQ. 2012. Gains or losses: molecular mechanisms of TDP43-mediated neurodegeneration. *Nature Reviews Neuroscience*, **13**(1): 38–50.

Lehmkuhl EM, Loganathan S, Alsop E, et al. 2021. TDP-43 proteinopathy alters the ribosome association of multiple mRNAs including the glypican Dally-like protein (Dlp)/GPC6. *Acta Neuropathologica Communications*, **9**(1): 52.

Li H, Wu SH, Ma X, et al. 2021. Co-editing *PINK1* and *DJ-1* genes *via* adeno-associated virus-delivered CRISPR/Cas9 system in adult monkey brain elicits classical parkinsonian phenotype. *Neuroscience Bulletin*, **37**(9): 1271–1288.

Li Q, Yokoshi M, Okada H, et al. 2015. The cleavage pattern of TDP-43 determines its rate of clearance and cytotoxicity. *Nature Communications*, **6**(1): 6183.

Li XJ, Lai LX. 2024. A booming field of large animal model research. *Zoological Research*, **45**(2): 311–313.

Li Y, Ray P, Rao EJ, et al. 2010. A *Drosophila* model for TDP-43 proteinopathy. *Proceedings of the National Academy of Sciences of the United States of America*, **107**(7): 3169–3174.

Majumder P, Chu JF, Chatterjee B, et al. 2016. Co-regulation of mRNA translation by TDP-43 and Fragile X Syndrome protein FMRP. *Acta Neuropathologica*, **132**(5): 721–738.

McAleese KE, Walker L, Erskine D, et al. 2017. TDP‐43 pathology in Alzheimer's disease, dementia with Lewy bodies and ageing. *Brain Pathology*, **27**(4): 472–479.

Mitchell JC, Constable R, So E, et al. 2015. Wild type human TDP-43 potentiates ALS-linked mutant TDP-43 driven progressive motor and cortical neuron degeneration with pathological features of ALS. *Acta Neuropathologica Communications*, **3**(1): 36.

Neelagandan N, Gonnella G, Dang S, et al. 2019. TDP-43 enhances translation of specific mRNAs linked to neurodegenerative disease. *Nucleic Acids Research*, **47**(1): 341–361.

Neumann M, Kwong LK, Sampathu DM, et al. 2007. TDP-43 proteinopathy in frontotemporal lobar degeneration and amyotrophic lateral sclerosis: protein misfolding diseases without amyloidosis. *Archives of Neurology*, **64**(10): 1388–1394.

Neumann M, Sampathu DM, Kwong LK, et al. 2006. Ubiquitinated TDP-43 in frontotemporal lobar degeneration and amyotrophic lateral sclerosis. *Science*, **314**(5796): 130–133.

Ni JX, Ren YF, Su TH, et al. 2023. Loss of TDP-43 function underlies hippocampal and cortical synaptic deficits in TDP-43 proteinopathies. *Molecular Psychiatry*, **28**(2): 931–945.

Nishimoto Y, Ito D, Yagi T, et al. 2010. Characterization of alternative isoforms and inclusion body of the TAR DNA-binding protein-43. *Journal of Biological Chemistry*, **285**(1): 608–619.

Nonaka T, Kametani F, Arai T, et al. 2009. Truncation and pathogenic mutations facilitate the formation of intracellular aggregates of TDP-43. *Human Molecular Genetics*, **18**(18): 3353–3364.

Pesiridis GS, Lee VMY, Trojanowski JQ. 2009. Mutations in TDP-43 link glycine-rich domain functions to amyotrophic lateral sclerosis. *Human Molecular Genetics*, **18**(R2): R156–R162.

Philips T, Rothstein JD. 2015. Rodent models of amyotrophic lateral sclerosis. *Current Protocols in Pharmacology*, **69**(1): 5.67. 1–5.67. 21.

Polymenidou M, Lagier-Tourenne C, Hutt KR, et al. 2011. Long pre-mRNA depletion and RNA missplicing contribute to neuronal vulnerability from loss of TDP-43. *Nature Neuroscience*, **14**(4): 459–468.

Prakash A, Kumar V, Banerjee A, et al. 2021. Structural heterogeneity in RNA recognition motif 2 (RRM2) of TAR DNA-binding protein 43 (TDP-43): clue to amyotrophic lateral sclerosis. *Journal of Biomolecular Structure and Dynamics*, **39**(1): 357–367.

Prpar Mihevc S, Darovic S, Kovanda A, et al. 2017. Nuclear trafficking in amyotrophic lateral sclerosis and frontotemporal lobar degeneration. *Brain*, **140**(1): 13–26.

Ratti A, Buratti E. 2016. Physiological functions and pathobiology of TDP‐43 and FUS/TLS proteins. *Journal of Neurochemistry*, **138**(S1): 95–111.

Renton AE, Chiò A, Traynor BJ. 2014. State of play in amyotrophic lateral sclerosis genetics. *Nature Neuroscience*, **17**(1): 17–23.

Russo A, Scardigli R, La Regina F, et al. 2017. Increased cytoplasmic TDP-43 reduces global protein synthesis by interacting with RACK1 on polyribosomes. *Human Molecular Genetics*, **26**(8): 1407–1418.

Shan X, Chiang PM, Price DL, et al. 2010. Altered distributions of Gemini of coiled bodies and mitochondria in motor neurons of *TDP-43* transgenic mice. *Proceedings of the National Academy of Sciences of the United*

*States of America*, **107**(37): 16325–16330.

Spiller KJ, Restrepo CR, Khan T, et al. 2018. Microglia-mediated recovery from ALS-relevant motor neuron degeneration in a mouse model of TDP-43 proteinopathy. *Nature Neuroscience*, **21**(3): 329–340.

Swarup V, Phaneuf D, Dupré N, et al. 2011. Deregulation of TDP-43 in amyotrophic lateral sclerosis triggers nuclear factor κB–mediated pathogenic pathways. *Journal of Experimental Medicine*, **208**(12): 2429–2447.

Ticozzi N, Leclerc AL, van Blitterswijk M, et al. 2011. Mutational analysis of *TARDBP* in neurodegenerative diseases. *Neurobiology of Aging*, **32**(11): 2096–2099.

Tsuiji H, Inoue I, Takeuchi M, et al. 2017. TDP-43 accelerates age-dependent degeneration of interneurons. *Scientific Reports*, **7**(1): 14972.

Uchida A, Sasaguri H, Kimura N, et al. 2012. Non-human primate model of amyotrophic lateral sclerosis with cytoplasmic mislocalization of TDP-43. *Brain*, **135**(3): 833–846.

Underwood W, Anthony R. 2020. AVMA guidelines for the euthanasia of animals: 2020 edition. *Retrieved on March*, **2013**(30): 2020–2021.

Voigt A, Herholz D, Fiesel FC, et al. 2010. TDP-43-mediated neuron loss *in vivo* requires RNA-binding activity. *PLoS One*, **5**(8): e12247.

Walker AK, Tripathy K, Restrepo CR, et al. 2015. An insoluble frontotemporal lobar degeneration-associated TDP-43 C-terminal fragment causes neurodegeneration and hippocampus pathology in transgenic mice. *Human Molecular Genetics*, **24**(25): 7241–7254.

Wang GH, Yang HQ, Yan S, et al. 2015. Cytoplasmic mislocalization of RNA splicing factors and aberrant neuronal gene splicing in TDP-43 transgenic pig brain. *Molecular Neurodegeneration*, **10**: 42.

Watanabe S, Oiwa K, Murata Y, et al. 2020. ALS-linked TDP-43$^{M337V}$ knock-in mice exhibit splicing deregulation without neurodegeneration. *Molecular Brain*, **13**(1): 8.

Wegorzewska I, Bell S, Cairns NJ, et al. 2009. TDP-43 mutant transgenic mice develop features of ALS and frontotemporal lobar degeneration. *Proceedings of the National Academy of Sciences of the United States of America*, **106**(44): 18809–18814.

Wils H, Kleinberger G, Janssens J, et al. 2010. TDP-43 transgenic mice develop spastic paralysis and neuronal inclusions characteristic of ALS and frontotemporal lobar degeneration. *Proceedings of the National Academy of Sciences of the United States of America*, **107**(8): 3858–3863.

Winton MJ, Igaz LM, Wong MM, et al. 2008. Disturbance of nuclear and cytoplasmic TAR DNA-binding protein (TDP-43) induces disease-like redistribution, sequestration, and aggregate formation. *Journal of Biological Chemistry*, **283**(19): 13302–13309.

Xu ZS, Yang CX. 2014. TDP-43—The key to understanding amyotrophic lateral sclerosis. *Rare Diseases*, **2**(1): e944443.

Yan S, Wang CE, Wei W, et al. 2014. TDP-43 causes differential pathology in neuronal versus glial cells in the mouse brain. *Human Molecular Genetics*, **23**(10): 2678–2693.

Yin P, Bai DZ, Deng FY, et al. 2022. SQSTM1-mediated clearance of cytoplasmic mutant TARDBP/TDP-43 in the monkey brain. *Autophagy*, **18**(8): 1955–1968.

Yin P, Guo XY, Yang WL, et al. 2019. Caspase-4 mediates cytoplasmic accumulation of TDP-43 in the primate brains. *Acta Neuropathologica*, **137**(6): 919–937.